Topic 9D - The Electronic Structure of d-Metal Complexes

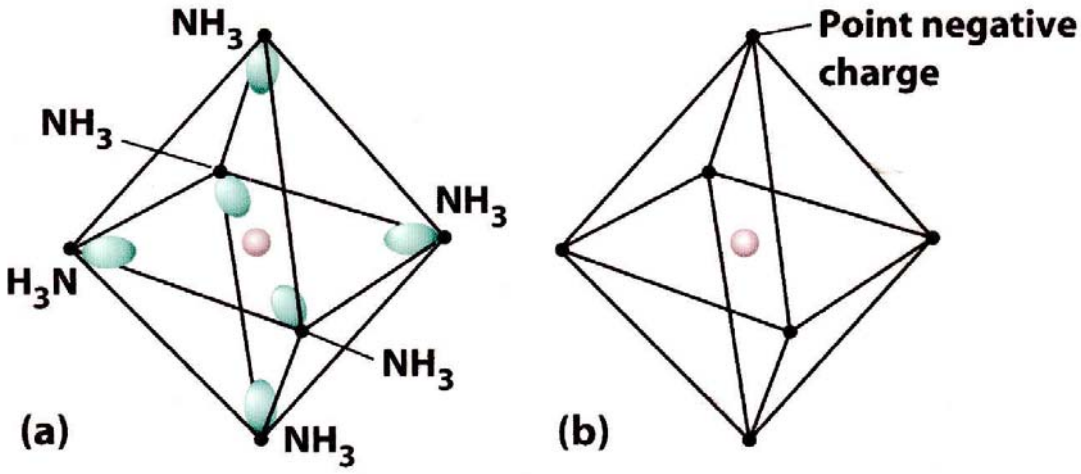

FIGURE 16.27 In the crystal field theory of complexes, the lone pairs of electrons that serve as the Lewis base sites on the ligands (a) are treated as equivalent to point negative charges (b).

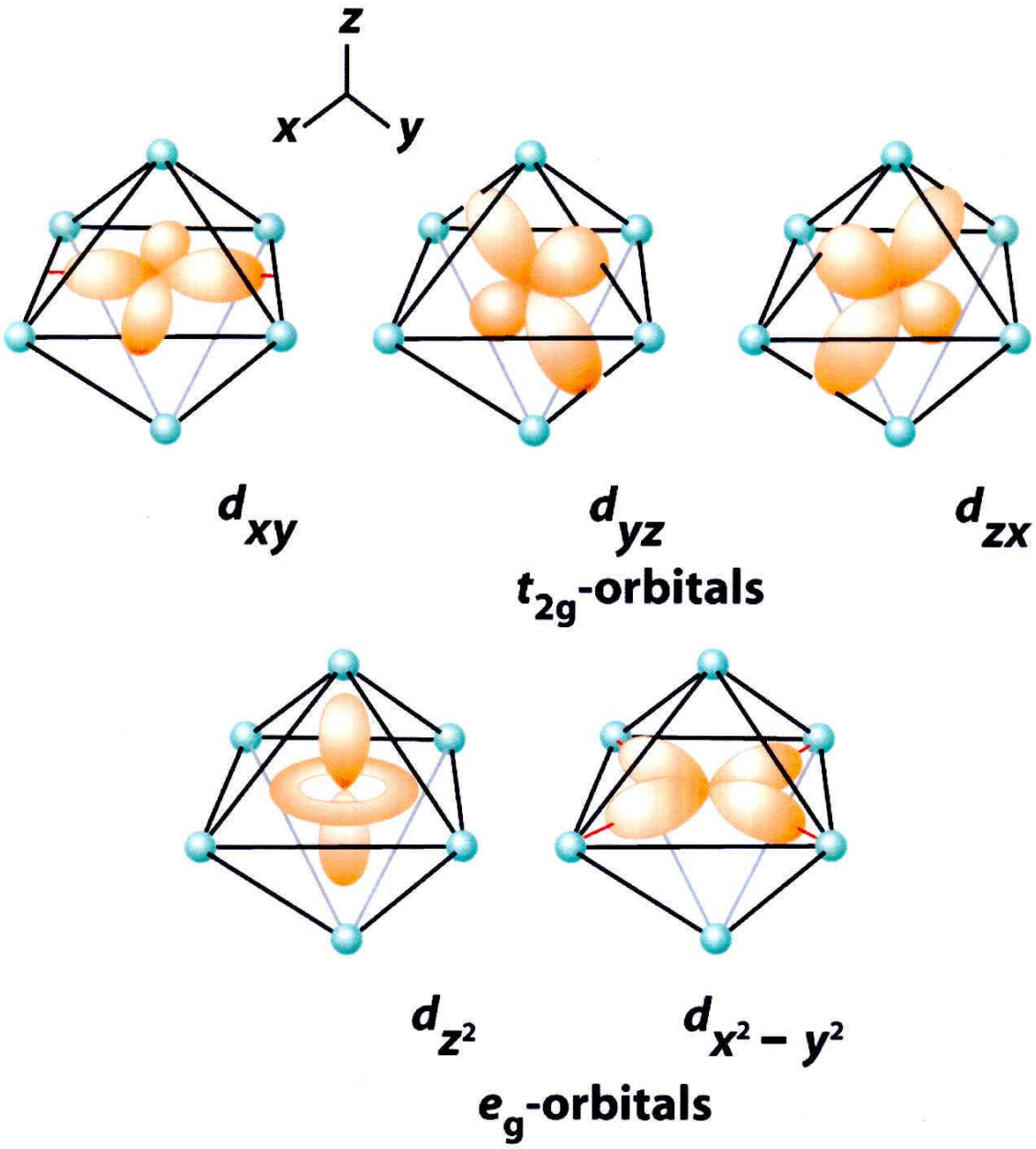

FIGURE 16.28 In an octahedral complex with a central *d*-metal atom or ion, a d_{xy}-orbital is directed between the ligand sites, and an electron that occupies it has a relatively low energy. The same lowering of energy occurs for d_{yz}- and d_{zx}-orbitals. A d_{z^2}-orbital points directly toward two ligands, and an electron that occupies it has a relatively high energy. The same rise in energy occurs for a $d_{x^2-y^2}$-electron.

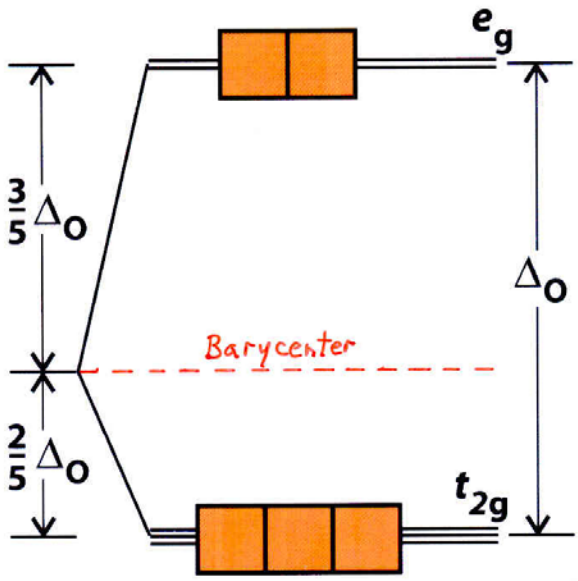

FIGURE 16.29 The energy levels of the *d*-orbitals in an octahedral complex with the ligand field splitting Δ_O. Each orbital (represented by a box) can hold two electrons. The center horizontal line on the far left represents the energy of the *d*-orbitals before complex formation.

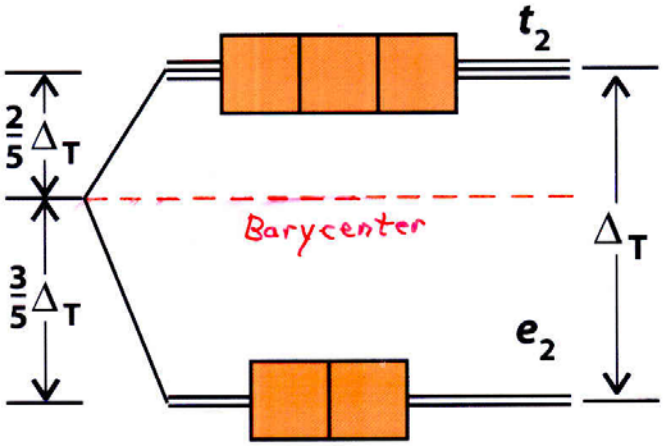

FIGURE 16.31 The energy levels of the *d*-orbitals in a tetrahedral complex with the ligand field splitting Δ_T. Each box (that is, orbital) can hold two electrons. The subscript g is not used to label the orbitals in a tetrahedral complex.

FIGURE 4.7

Eight ligands of a cubic field surrounding a central metal atom or ion. The ligands in bold print represent one of the two tetrahedra that together constitute the cubic field. The Cartesian axes project from each face of the cube.

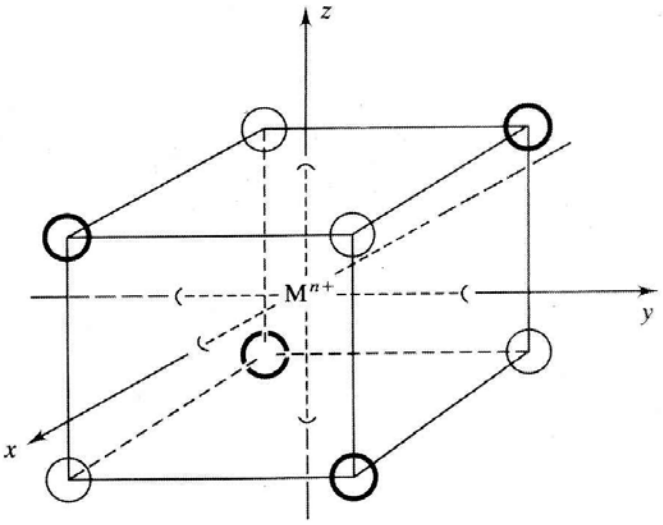

FIGURE 4.8

The five *d* orbitals of a metal atom or ion in a tetrahedral field. The top three orbitals (d_{xy}, d_{xz}, and d_{yz}) are a distance $l/2$ from the ligands, and the bottom two ($d_{z^2-y^2}$ and d_{z^2}) are farther away at $l\sqrt{2}/2$. l is defined as the length of the cube edge.

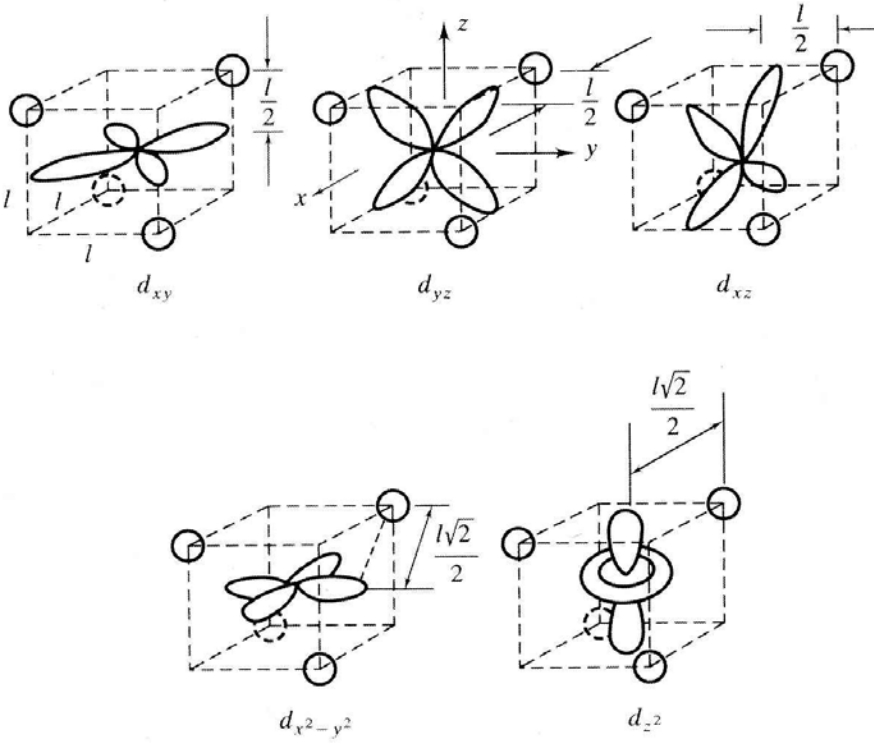

FIGURE 4.9

The crystal field splitting of the *d* orbitals by a tetrahedral field.

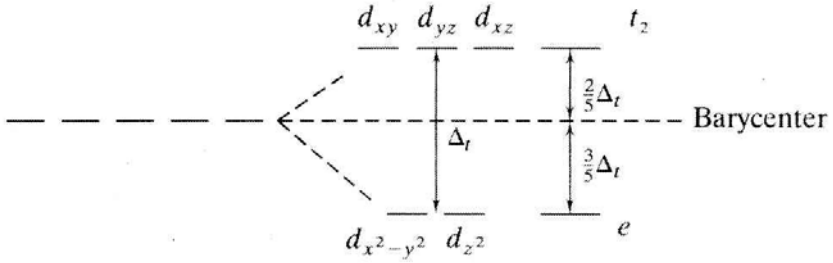

$$\Delta_t \approx \tfrac{4}{9}\Delta_0$$

FIGURE 4.5

Structural and energy changes in the formation of an octahedral field. (*a*) Four hypothetical stages of the construction of an octahedral field about a metal cation and (*b*) the energies of the *d* orbitals corresponding to each stage. Note that the relative energy changes are not to scale. The split between the *d* orbitals is actually much smaller than the energy changes in going from stages I to II or III to IV. (From Audrey Companion, *Chemical Bonding*, pp. 150–151, Copyright © 1979. McGraw-Hill.)

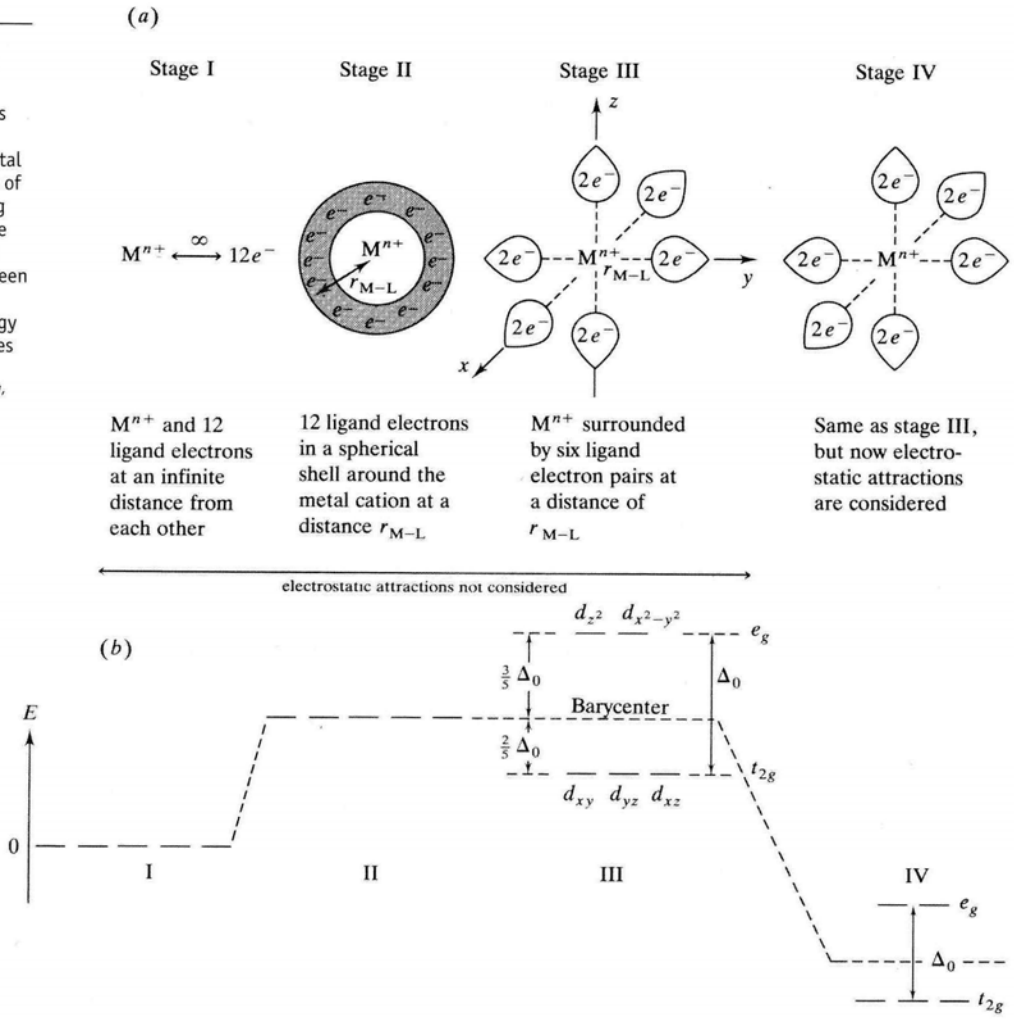

FIGURE 4.6

Structural and energy changes in the conversion of an octahedral field to a square planar field.
(*a*) The gradual removal of the *z*-axis ligands results in the progression from an octahedral to a tetragonally elongated octahedral to a square planar field of ligands. (*b*) The change in the energies of the *d* orbitals in a central metal atom or ion corresponding to the three fields. (From F.A. Cotton and G.Wilkinson, *Advanced Inorganic Chemistry*, 4th ed., Copyright © 1980. Reprinted by permission of John Wiley & Sons, Inc.)

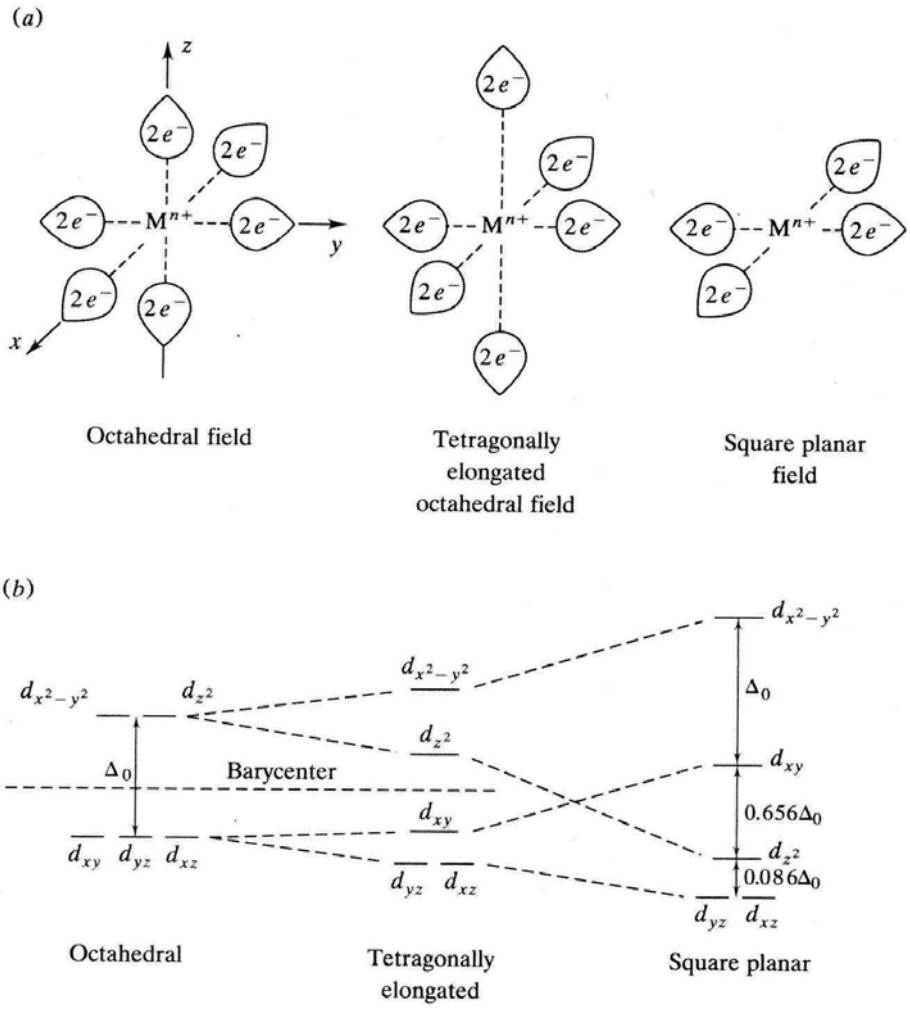

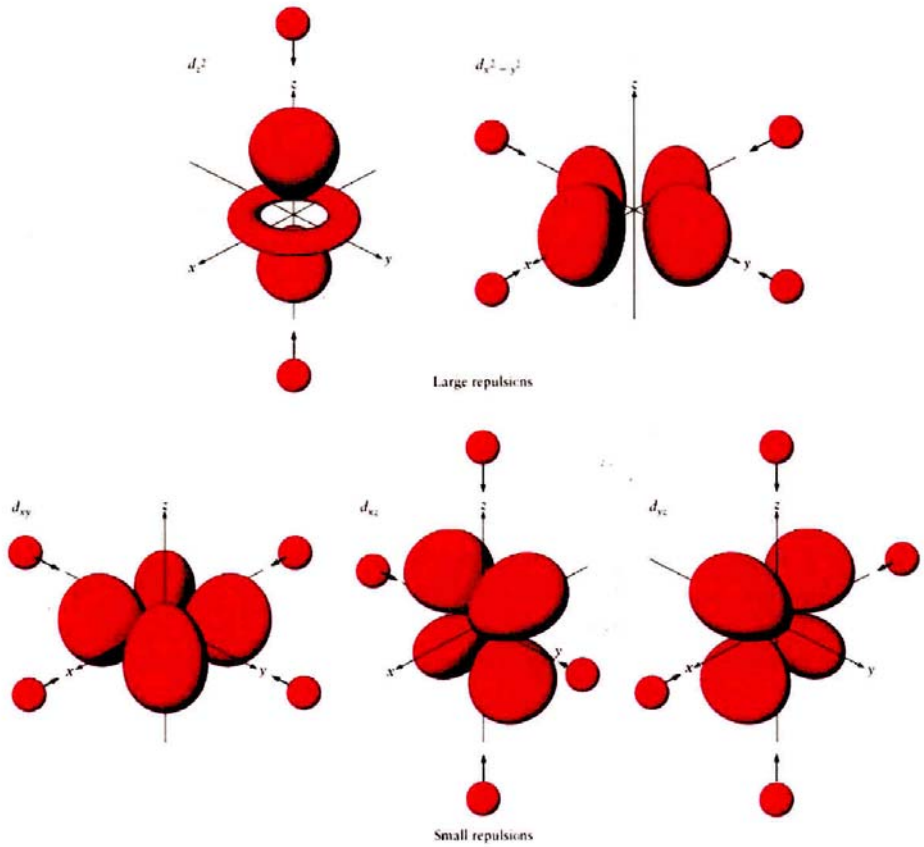

FIGURE 8.24 The basis for octahedral crystal field splitting of 3*d*-orbital energies by ligands. As the external charges approach the five 3*d* orbitals, the largest repulsions arise in the d_{z^2} and $d_{x^2-y^2}$ orbitals, which point directly at two or four of the approaching charges. External charges that have negligible interactions with the *d* electrons are not shown.

FIGURE 8.25 An octahedral field increases the energies of all five *d* orbitals, but the increase is greater for the d_{z^2} and $d_{x^2-y^2}$ orbitals. As a result, the orbitals are split into two sets that differ by the energy Δ_o. The orbital occupancy shown is for (a) the high-spin (small Δ_o) and (b) the low-spin (large Δ_o) complexes of Mn(III).

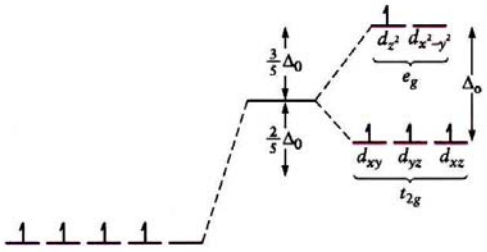

(a) $[Mn(H_2O)_6]^{3+}$ (high spin)

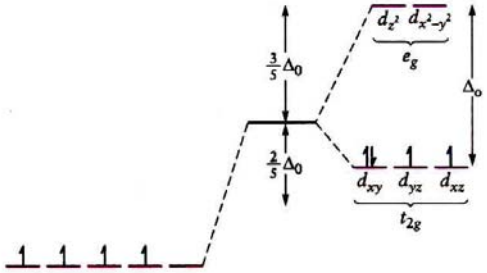

(b) $[Mn(CN)_6]^{3-}$ (low spin)

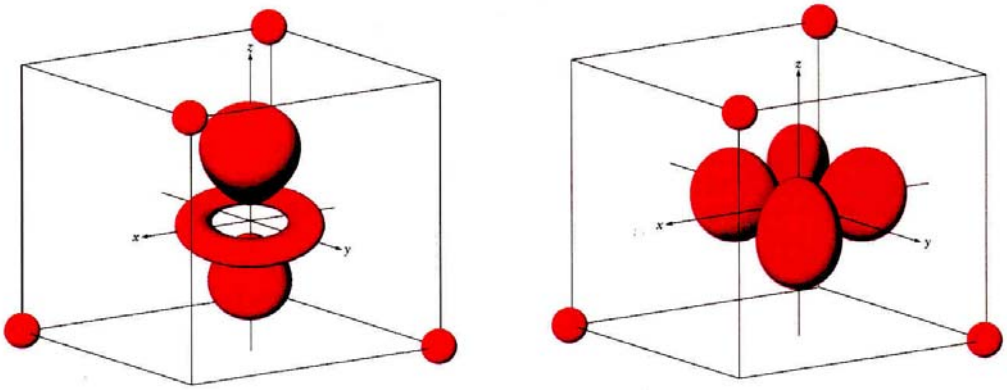

FIGURE 8.26 Energy-level structures of the 3*d* orbitals in square-planar and tetrahedral crystal fields.

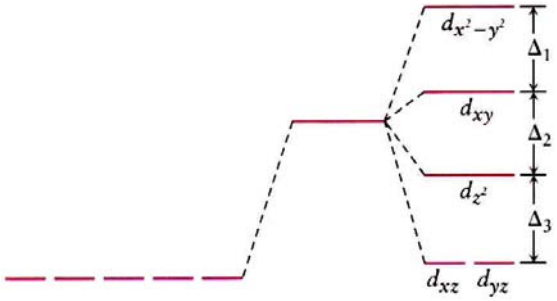

(a) Square planar

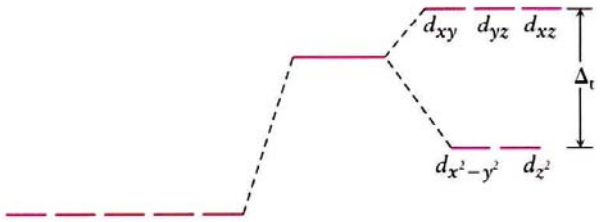

(b) Tetrahedral

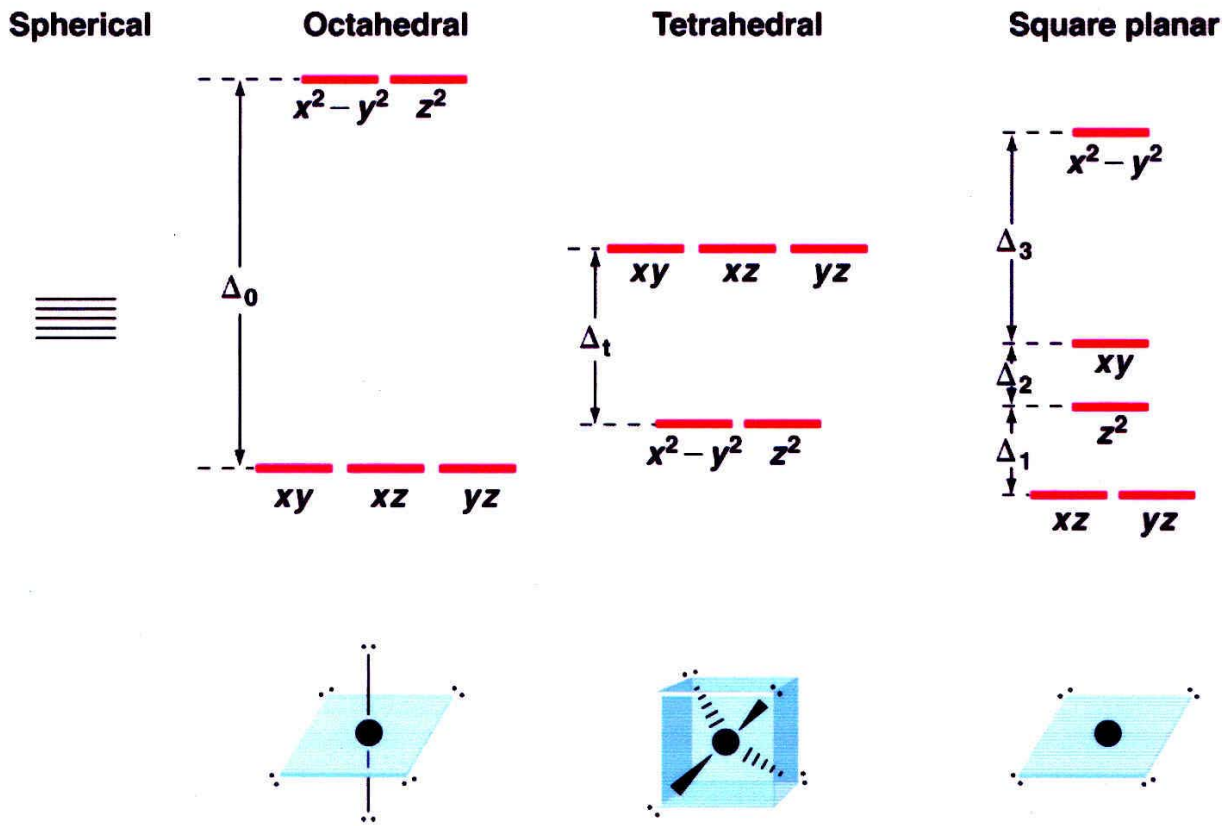
Spherical
Octahedral
Tetrahedral
Square planar
$x^2 - y^2$
z^2
Δ_0
xy
xz
yz
Δ_t
Δ_3
Δ_2
Δ_1

FIGURE 16.32 The spectrochemical series. Strong-field ligands give rise to a large splitting between the *t*- and *e*-orbitals, whereas weak-field ligands give rise to only a small splitting. The horizontal line marks the approximate frontier between the two kinds of ligands. The changing color represents the increasing energy of light absorbed as the field strength increases.

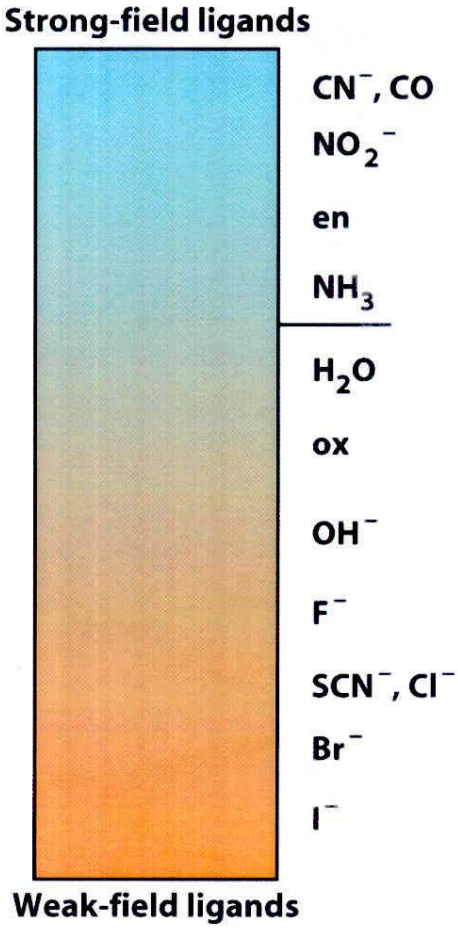

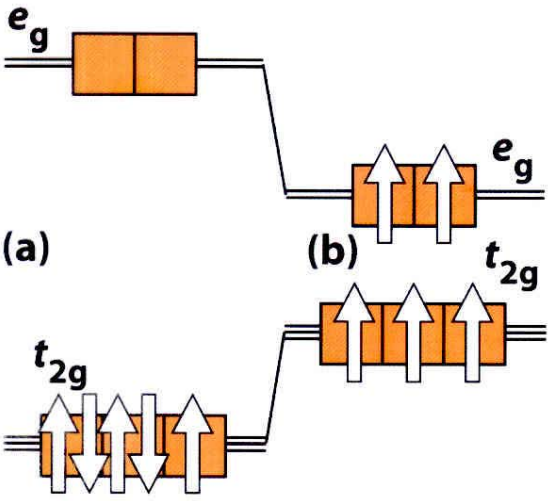

FIGURE 16.37 (a) A strong-field ligand is likely to lead to a low-spin complex (in this case, the configuration is that of Fe^{3+}). (b) Substituting weak-field ligands is likely to result in a high-spin complex.

Crystal Field Splitting – Magnitude of Δ

3. Nature of ligand – Spectrochemical series

$I^- < Br^- < OCrO_3^{2-}$ chromate $< Cl^- \approx SCN^- < N_3^- <$
$F^- \approx SSO_3^{2-}$ thiosulfate $\approx$ **urea** (O) $< OCO_2^{2-}$ carbonate $<$
OCO_2R^- carboxylate $< ONO^- \approx OH^- < OSO_3^{2-}$ sulfate $<$
ONO_2^- nitrate $< O_2CCO_2^{2-}$ oxalate (bidentate) $< H_2O <$
$NCS^- <$ **glycine** $\approx EDTA^{4-} <$ **pyidine** $\approx NH_3 <$ **en** $<$
$SO_3^{2-} <$ **bipy** $<$ ***o*-phen** $< NO_2^- <$ **Cp** $< CN^-$

X weak field
O middle
N strong field
C very strong

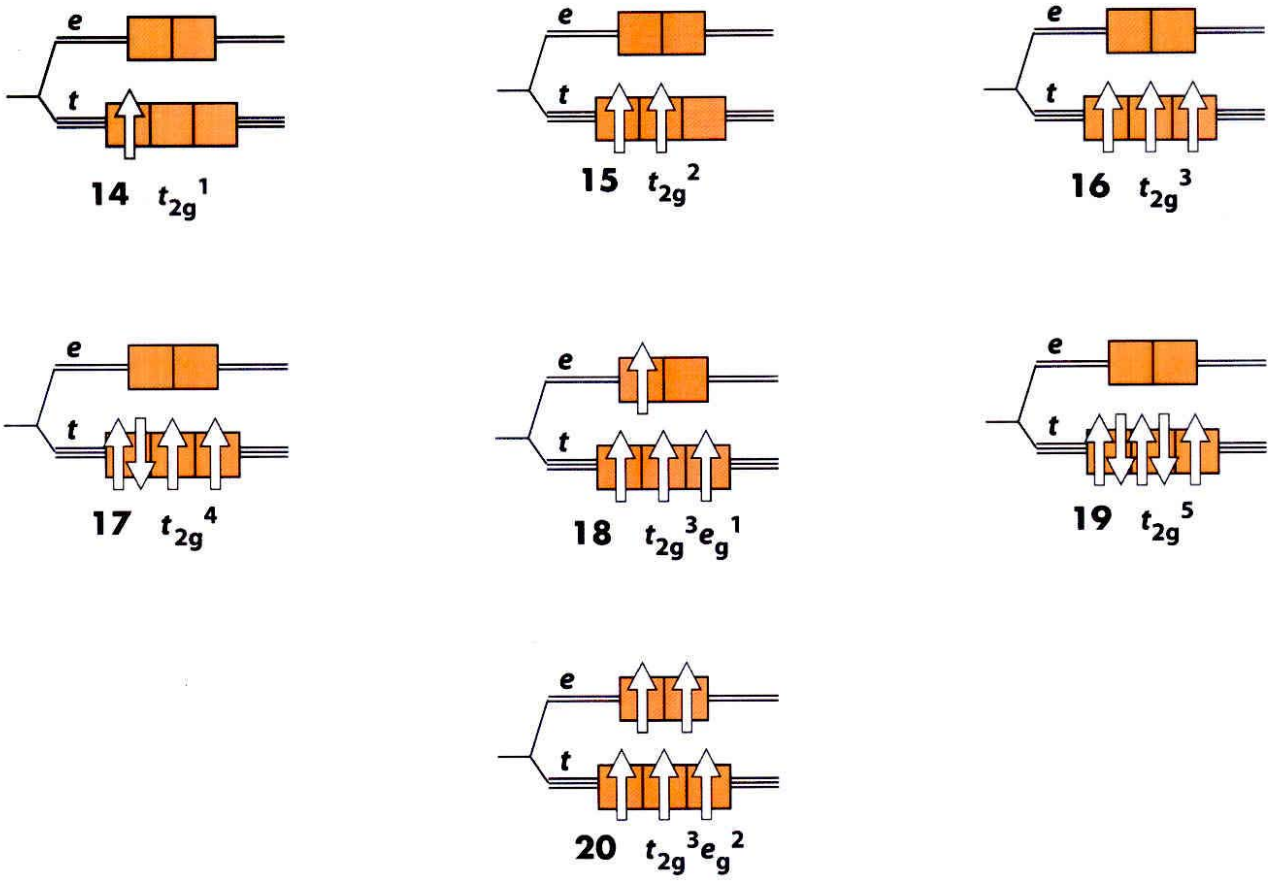

TABLE 16.5 Electron Configurations of d^n Complexes

Number of *d*-electrons	Configuration		
	Octahedral complexes		Tetrahedral complexes
d^1	t_{2g}^{1}		e^1
d^2	t_{2g}^{2}		e^2
d^3	t_{2g}^{3}		$e^2t_2^{1}$
	Low spin	High spin	
d^4	t_{2g}^{4}	$t_{2g}^{3}e_g^{1}$	$e^2t_2^{2}$
d^5	t_{2g}^{5}	$t_{2g}^{3}e_g^{2}$	$e^2t_2^{3}$
d^6	t_{2g}^{6}	$t_{2g}^{4}e_g^{2}$	$e^3t_2^{3}$
d^7	$t_{2g}^{6}e_g^{1}$	$t_{2g}^{5}e_g^{2}$	$e^4t_2^{3}$
d^8	$t_{2g}^{6}e_g^{2}$		$e^4t_2^{4}$
d^9	$t_{2g}^{6}e_g^{3}$		$e^4t_2^{5}$
d^{10}	$t_{2g}^{6}e_g^{4}$		$e^4t_2^{6}$

TABLE 8.5 Electron Configurations and Crystal Field Stabilization Energies for High- and Low-Spin Octahedral Complexes

Configuration		d^1	d^2	d^3	d^4	d^5	d^6	d^7	d^8	d^9	d^{10}
Examples		Ti^{3+}	Ti^{2+}, V^{3+}	V^{2+}, Cr^{3+}	Mn^{3+}, Re^{3+}	Mn^{2+}, Fe^{3+}	Fe^{2+}, Pd^{4+}	Co^{2+}, Rh^{2+}	Ni^{2+}, Pt^{2+}	Cu^{2+}	Zn^{2+}, Ag^{+}
HIGH SPIN	e_g				↑	↑ ↑	↑ ↑	↑ ↑	↑ ↑	↑↓ ↑	↑↓ ↑↓
	t_{2g}	↑	↑ ↑	↑ ↑ ↑	↑ ↑ ↑	↑ ↑ ↑	↑↓ ↑ ↑	↑↓ ↑↓ ↑	↑↓ ↑↓ ↑↓	↑↓ ↑↓ ↑↓	↑↓ ↑↓ ↑↓
	CFSE	$-\frac{2}{5}\Delta_o$	$-\frac{4}{5}\Delta_o$	$-\frac{6}{5}\Delta_c$	$-\frac{3}{5}\Delta_o$	0	$-\frac{2}{5}\Delta_o$	$-\frac{4}{5}\Delta_o$	$-\frac{6}{5}\Delta_o$	$-\frac{3}{5}\Delta_o$	0
LOW SPIN	e_g							↑			
	t_{2g}				↑↓ ↑ ↑	↑↓ ↑↓ ↑	↑↓ ↑↓ ↑↓	↑↓ ↑↓ ↑↓			
	CFSE	Same as high spin			$-\frac{8}{5}\Delta_o$	$-\frac{10}{5}\Delta_o$	$-\frac{12}{5}\Delta_o$	$-\frac{3}{5}\Delta_o$	Same as high spin		

Color Wheel

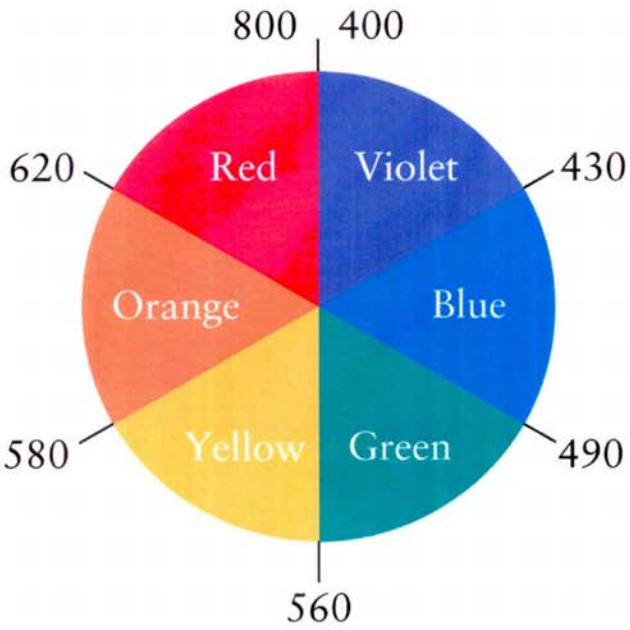

In a color wheel the color of light absorbed is opposite the color perceived. For example, a complex that absorbs orange light appears blue.

Colors of Co (III) Complexes

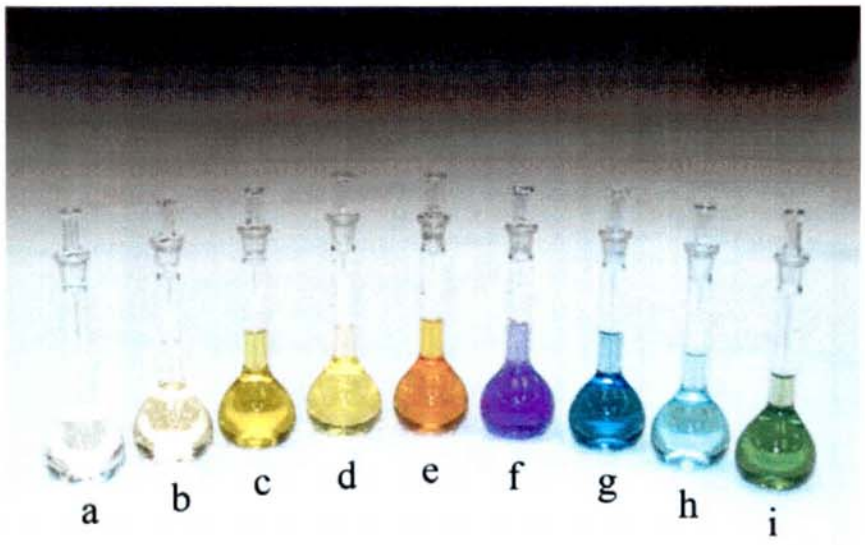

Figure 2. Photograph of solutions produced in the current experiment. Solutions are ordered according to the ligand spectrochemical series: (a) CN^-, (b) NO_2^-, (c) phen, (d) en, (e) NH_3, (f) gly, (g) H_2O, (h) ox^{2-}, (i) CO_3^{2-}.

FIGURE 17.35 The effect on the color of the complex of substituting ligands with different ligand field strengths in octahedral cobalt(III) complexes in aqueous solution.

FIGURE 8.29 The colors of the hexaaqua complexes of metal ions (from left) Mn^{2+}, Fe^{3+}, Co^{2+}, Ni^{2+}, Cu^{2+}, and Zn^{2+}, prepared from their nitrate salts. Note that the d^{10} Zn^{2+} complex is colorless. The green color of the Ni^{2+} is due to absorption of both red and blue light that passes through the solution. The yellow color of the solution containing $Fe(H_2O)_6^{3+}$ is caused by hydrolysis of that ion to form $Fe(OH)(H_2O)_5^{2+}$; if this reaction is suppressed, the solution is pale violet.

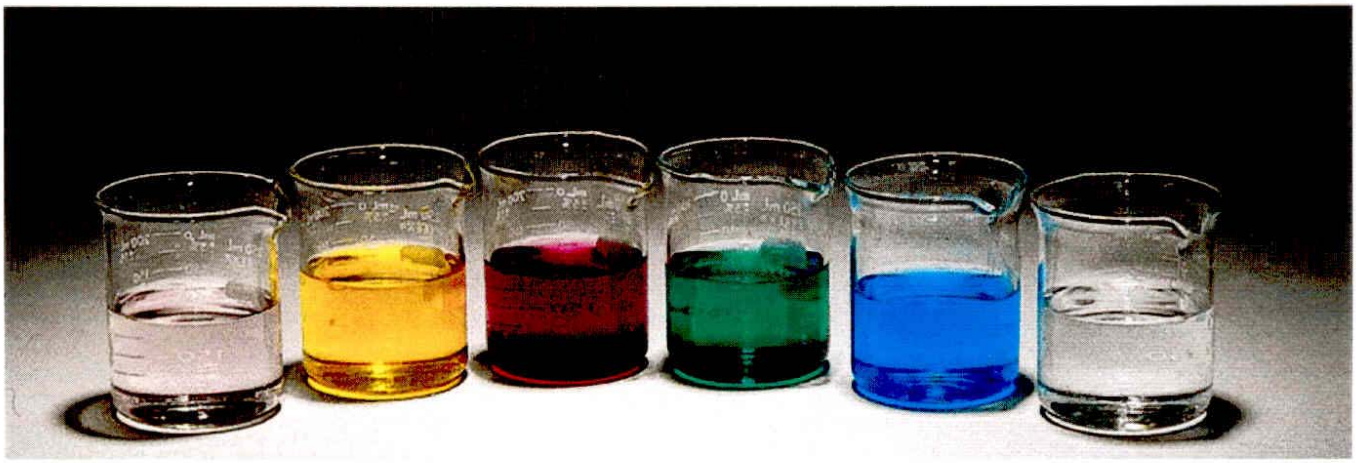

TABLE 8.6 Absorption Wavelengths for Selected Octahedral Transition-Metal Complexes

Octahedral Complexes		λ_{max} (nm)	Octahedral Complexes		λ_{max} (nm)
$[TiF_6]^{3-}$		588	$[Co(NH_3)_6]^{3+}$	Yellow	437
$[Ti(H_2O)_6]^{3+}$		492	$[Co(CN)_6]^{3-}$		290
$[V(H_2O)_6]^{3+}$		560	$[Co(H_2O)_6]^{2+}$		1075
$[V(H_2O)_6]^{2+}$		806	$[Ni(H_2O)_6]^{2+}$	Green	1176
$[Cr(H_2O)_6]^{3+}$		575	$[Ni(NH_3)_6]^{2+}$		926
$[Cr(NH_3)_6]^{3+}$	Yellow	463	$[RhBr_6]^{3-}$		463
$[Cr(CN)_6]^{3-}$		376	$[RhCl_6]^{3-}$		439
$Cr(CO)_6$	Colorless	311	$[Rh(NH_3)_6]^{3+}$		293
$[Fe(CN)_6]^{3-}$	Red	310	$[Rh(CN)_6]^{3-}$		227
$[Fe(CN)_6]^{4-}$		296	$[IrCl_6]^{3-}$		362
$[Co(H_2O)_6]^{3+}$	Purple	549	$[Ir(NH_3)_6]^{3+}$	Colorless	250

Color [edit]

Metal complexes often have spectacular colors caused by electronic transitions by the absorption of light. For this reason they are often applied as pigments. Most transitions that are related to colored metal complexes are either **d-d transitions** or **charge transfer bands**. In a d-d transition, an electron in a d orbital on the metal is excited by a photon to another d orbital of higher energy. A charge transfer band entails promotion of an electron from a metal-based orbital into an empty ligand-based orbital (Metal-to-Ligand Charge Transfer or MLCT). The converse also occurs: excitation of an electron in a ligand-based orbital into an empty metal-based orbital (Ligand to Metal Charge Transfer or LMCT). These phenomena can be observed with the aid of electronic spectroscopy; also known as UV-Vis.[9] For simple compounds with high symmetry, the d-d transitions can be assigned using Tanabe-Sugano diagrams. These assignments are gaining increased support with computational chemistry.

Colours of Various Example Coordination Complexes

	Fe^{II}	Fe^{III}	Co^{II}	Cu^{II}	Al^{III}	Cr^{III}
Hydrated Ion	$[Fe(H_2O)_6]^{2+}$ Pale green Soln	$[Fe(H_2O)_6]^{3+}$ Yellow/brown Soln	$[Co(H_2O)_6]^{2+}$ Pink Soln	$[Cu(H_2O)_6]^{2+}$ Blue Soln	$[Al(H_2O)_6]^{3+}$ Colourless Soln	$[Cr(H_2O)_6]^{3+}$ Green Soln
OH^-, dilute	$[Fe(H_2O)_4(OH)_2]$ Dark green Ppt	$[Fe(H_2O)_3(OH)_3]$ Brown Ppt	$[Co(H_2O)_4(OH)_2]$ Blue/green Ppt	$[Cu(H_2O)_4(OH)_2]$ Blue Ppt	$[Al(H_2O)_3(OH)_3]$ White Ppt	$[Cr(H_2O)_3(OH)_3]$ Green Ppt
OH^-, concentrated	$[Fe(H_2O)_4(OH)_2]$ Dark green Ppt	$[Fe(H_2O)_3(OH)_3]$ Brown Ppt	$[Co(H_2O)_4(OH)_2]$ Blue/green Ppt	$[Cu(H_2O)_4(OH)_2]$ Blue Ppt	$[Al(OH)_4]^-$ Colourless Soln	$[Cr(OH)_6]^{3-}$ Green Soln
NH_3, dilute	$[Fe(H_2O)_4(OH)_2]$ Dark green Ppt	$[Fe(H_2O)_3(OH)_3]$ Brown Ppt	$[Co(H_2O)_4(OH)_2]$ Blue/green Ppt	$[Cu(H_2O)_4(OH)_2]$ Blue Ppt	$[Al(H_2O)_3(OH)_3]$ White Ppt	$[Cr(H_2O)_3(OH)_3]$ Green Ppt
NH_3, concentrated	$[Fe(H_2O)_4(OH)_2]$ Dark green Ppt	$[Fe(H_2O)_3(OH)_3]$ Brown Ppt	$[Co(NH_3)_6]^{2+}$ Straw coloured Soln	$[Cu(NH_3)_4(H_2O)_2]^{2+}$ Deep blue Soln	$[Al(H_2O)_3(OH)_3]$ White Ppt	$[Cr(NH_3)_6]^{3+}$ Green Soln
CO_3^{2-}	$FeCO_3$ Dark green Ppt	$[Fe(H_2O)_3(OH)_3]$ Brown Ppt + bubbles	$CoCO_3$ Pink Ppt	$CuCO_3$ Blue/green Ppt		

Table 17.1: The "Eyeball Spectroscopy" Table for Broadband Electronic Absorption

TABLE 17.1

The "eyeball spectroscopy" table for broadband electronic absorption

Color you see	Color absorbed	Wavelength λ at band center (nm)	Energy level difference $\Delta E/hc$ (cm^{-1})
Colorless	Ultraviolet	<400	>25,000
Lemon yellow	Violet	410	24,400
Yellow	Indigo	430	23,200
Orange	Blue	480	20,800
Red	Blue-green	500	20,000
Purple	Green	530	18,900
Violet	Lemon yellow	560	17,900
Indigo	Yellow	580	17,300
Blue	Orange	610	16,400
Blue-green	Red	680	14,700
Green	Purple-red	720	13,900
Yellow-green	Purple	750	13,300

Tris(1,10-phenantholine)iron(II)

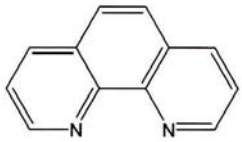

1,10-Phenanthroline

Fe^{2+} + 3phen → $(phen)_3Fe(II)$

orange-red complex

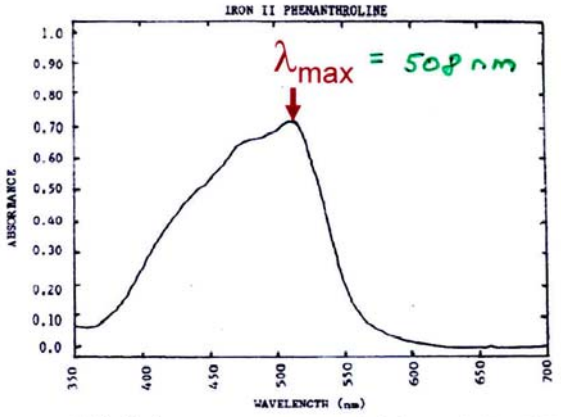

Visible spectrum of $(phen)_3Fe(II)$

TABLE 4.2

Octahedral Crystal Field Splitting Energies Δ_o, cm^{-1}

$(M')^{2+}$		$(M')^{3+}$		$(M'')^{3+}$		$(M''')^{3+}$	
			Cr^{2+}, Cr^{3+}, Mo^{3+}				
$[CrCl_6]^{4-}$	13,000	$[CrCl_6]^{3-}$	13,200	$[MoCl_6]^{3-}$	19,200		
$[Cr(H_2O)_6]^{2+}$	14,000	$[Cr(H_2O)_6]^{3+}$	17,400				
		$[Cr(NH_3)_6]^{3+}$	21,500				
$[Cr(en)_3]^{2+}$	18,000	$[Cr(en)_3]^{3+}$	21,900				
		$[Cr(CN)_6]^{3-}$	26,600				
			Co^{2+}, Co^{3+}, Rh^{3+}, Ir^{3+}				
				$[RhCl_6]^{3-}$	20,000	$[IrCl_6]^{3-}$	25,000
$[Co(H_2O)_6]^{2+}$	9,300	$[Co(H_2O)_6]^{3+}$	18,200	$[Rh(H_2O)_6]^{3+}$	27,000		
$[Co(NH_3)_6]^{2+}$	10,100	$[Co(NH_3)_6]^{3+}$	22,900	$[Rh(NH_3)_6]^{3+}$	34,100	$[Ir(NH_3)_6]^{3+}$	41,000
$[Co(en)_3]^{2+}$	11,000	$[Co(en)_3]^{3+}$	23,200	$[Rh(en)_3]^{3+}$	34,600	$[Ir(en)_3]^{3+}$	41,400
		$[Co(CN)_6]^{3-}$	33,500	$[Rh(CN)_6]^{3-}$	45,500		
			Mn^{2+}, Mn^{3+}				
$[MnCl_6]^{4-}$	7,500	$[MnCl_6]^{3-}$	20,000				
$[Mn(H_2O)_6]^{2+}$	8,500	$[Mn(H_2O)_6]^{3+}$	21,000				
$[Mn(en)_3]^{2+}$	10,100						
			Fe^{2+}, Fe^{3+}				
		$[FeCl_6]^{3-}$	11,000				
$[Fe(H_2O)_6]^{2+}$	8,500	$[Fe(H_2O)_6]^{3+}$	14,300				
$[Fe(CN)_6]^{4-}$	32,800	$[Fe(CN)_6]^{3-}$	35,000				

TABLE 17.4

A tale of two complexes

Complex	Color	Δ_o (cm^{-1})	Unpaired spins	K_f
CoF_6^{3-}	Yellow-green	13,000	4	$\ll 1$
$Co(NH_3)_6^{3+}$	Orange	22,900	0	1×10^{35}

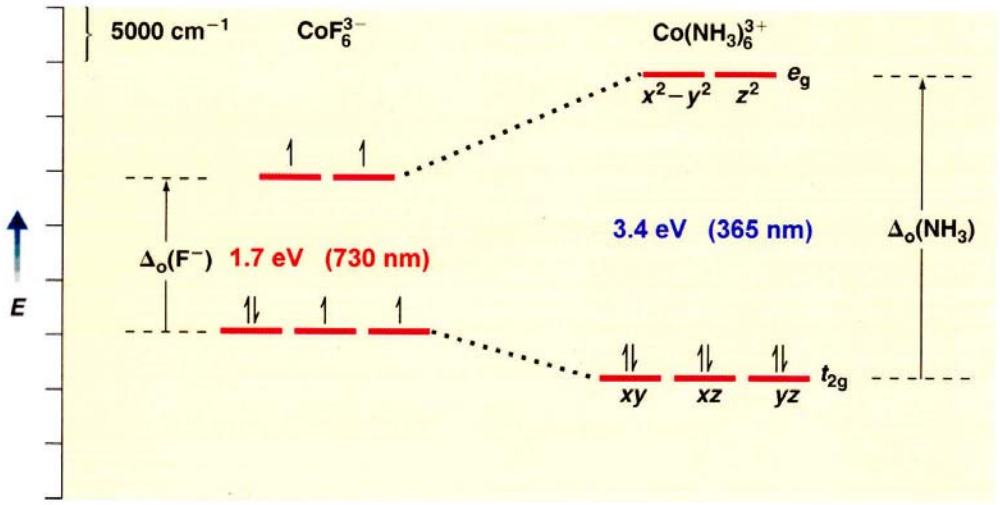

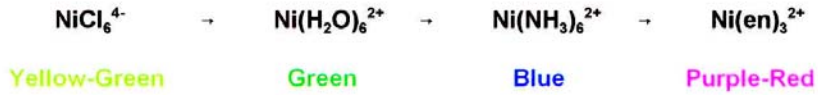

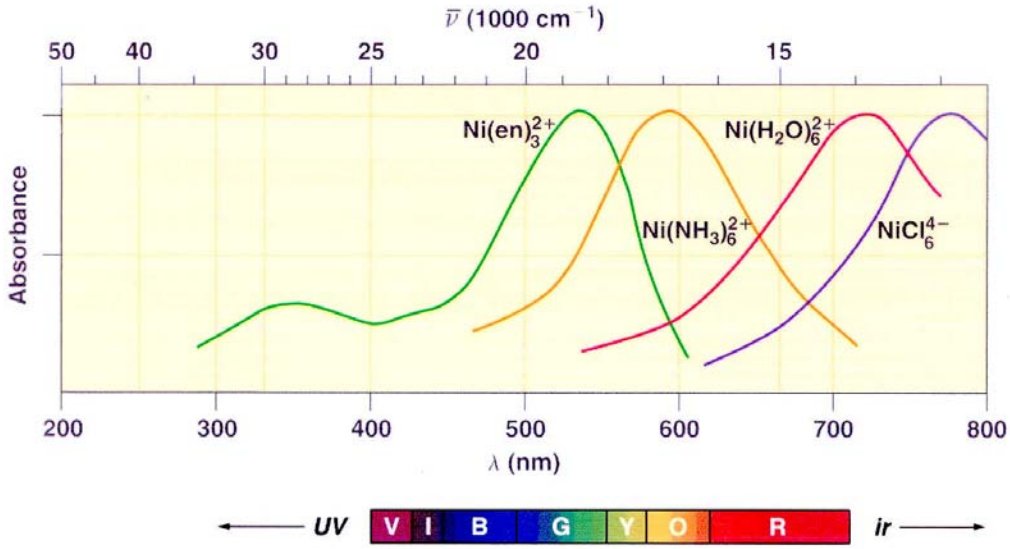

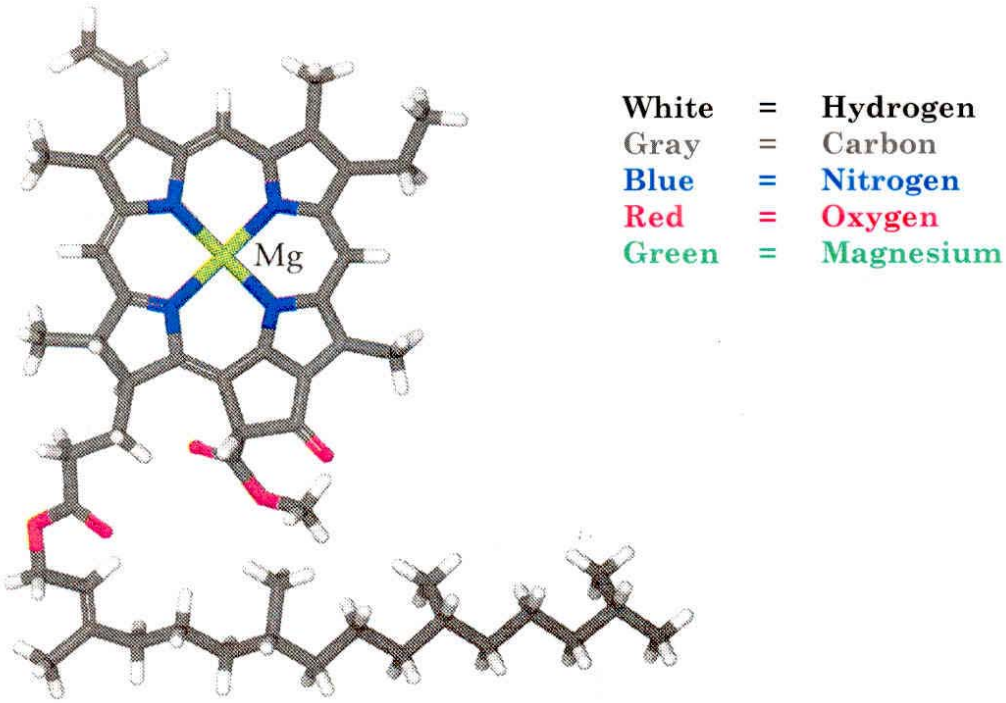

5 Chlorophyll - **a**

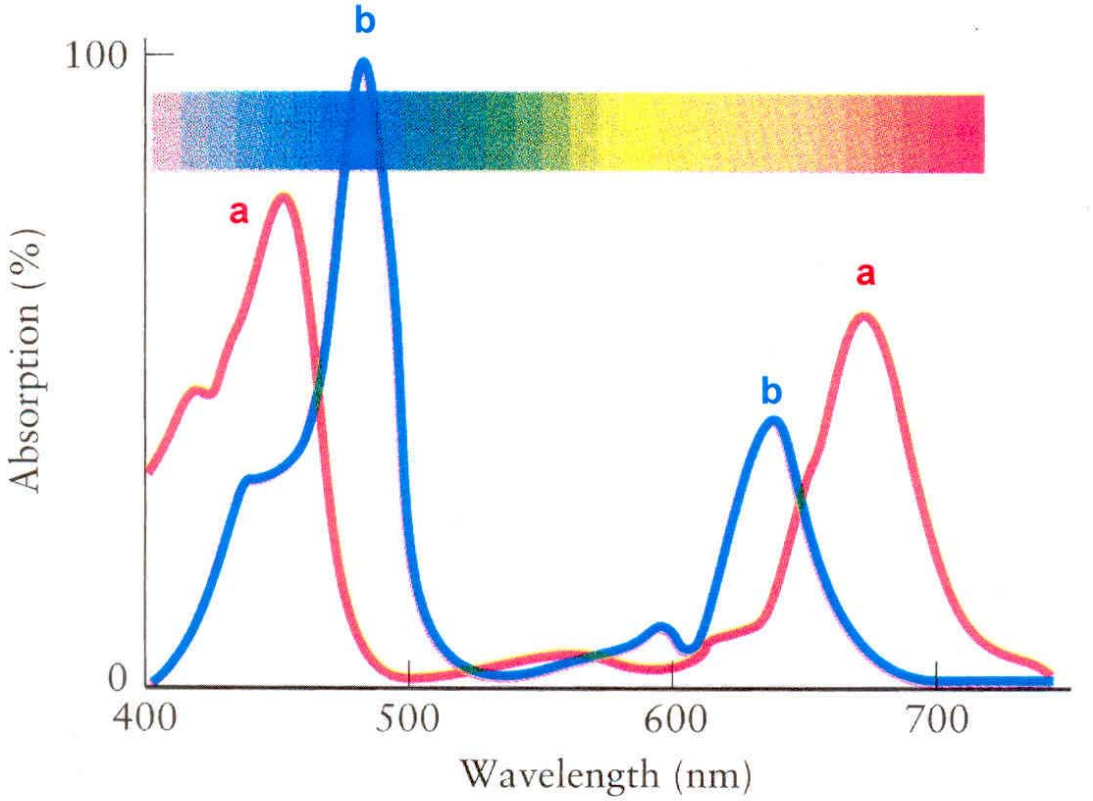

FIGURE 1 The optical absorption spectrum of chlorophyll as a plot of percentage absorption against wavelength. Chlorophyll *a* is shown in red, chlorophyll *b* in blue.

Chlorophyll-a

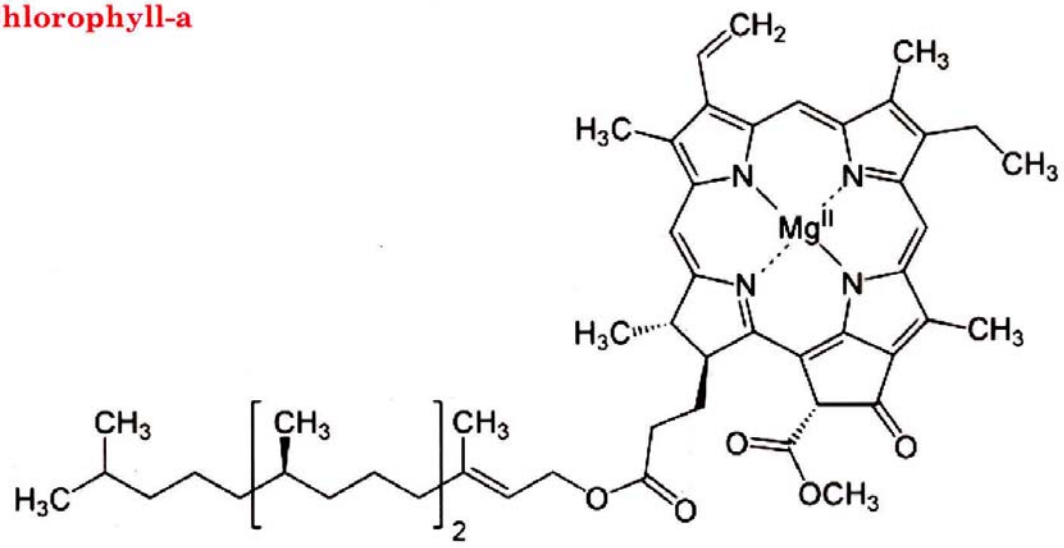

Chlorophyll-b

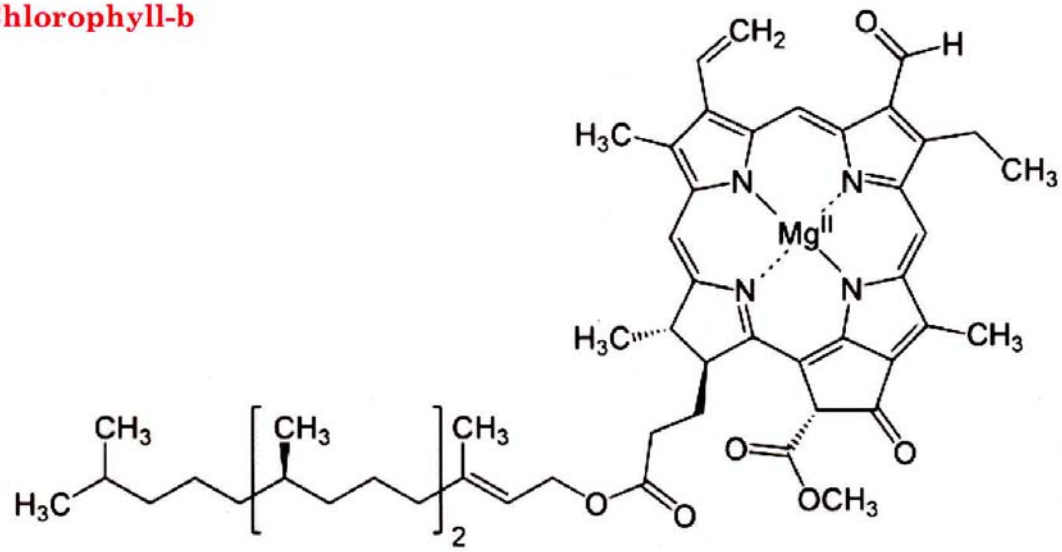

TABLE 8.7 Examples of Hybrid Orbitals and Bonding in Complexes

Coordination Number	Hybrid Orbital	Configuration	Examples	
2	*sp*	Linear	$[Ag(NH_3)_2]^+$	
3	sp^2	Trigonal planar	BF_3, NO_3^-, $[Ag(R_3P)_3]^+$	
4	sp^3	Tetrahedral	$Ni(CO)_4$, $[MnO_4]^-$, $[Zn(NH_3)_4]^{2+}$	
4	dsp^2	Planar	$[Ni(CN)_4]^{2-}$, $[Pt(NH_3)_4]^{2+}$	d^8
5	dsp^3	Trigonal bipyramid	TaF_5, $[CuCl_5]^{3-}$, $[Ni(PEt_3)_2Br_3]$	d^9
6	d^2sp^3	Octahedral	$[Co(NH_3)_6]^{3+}$, $[PtCl_6]^{2-}$	d^6

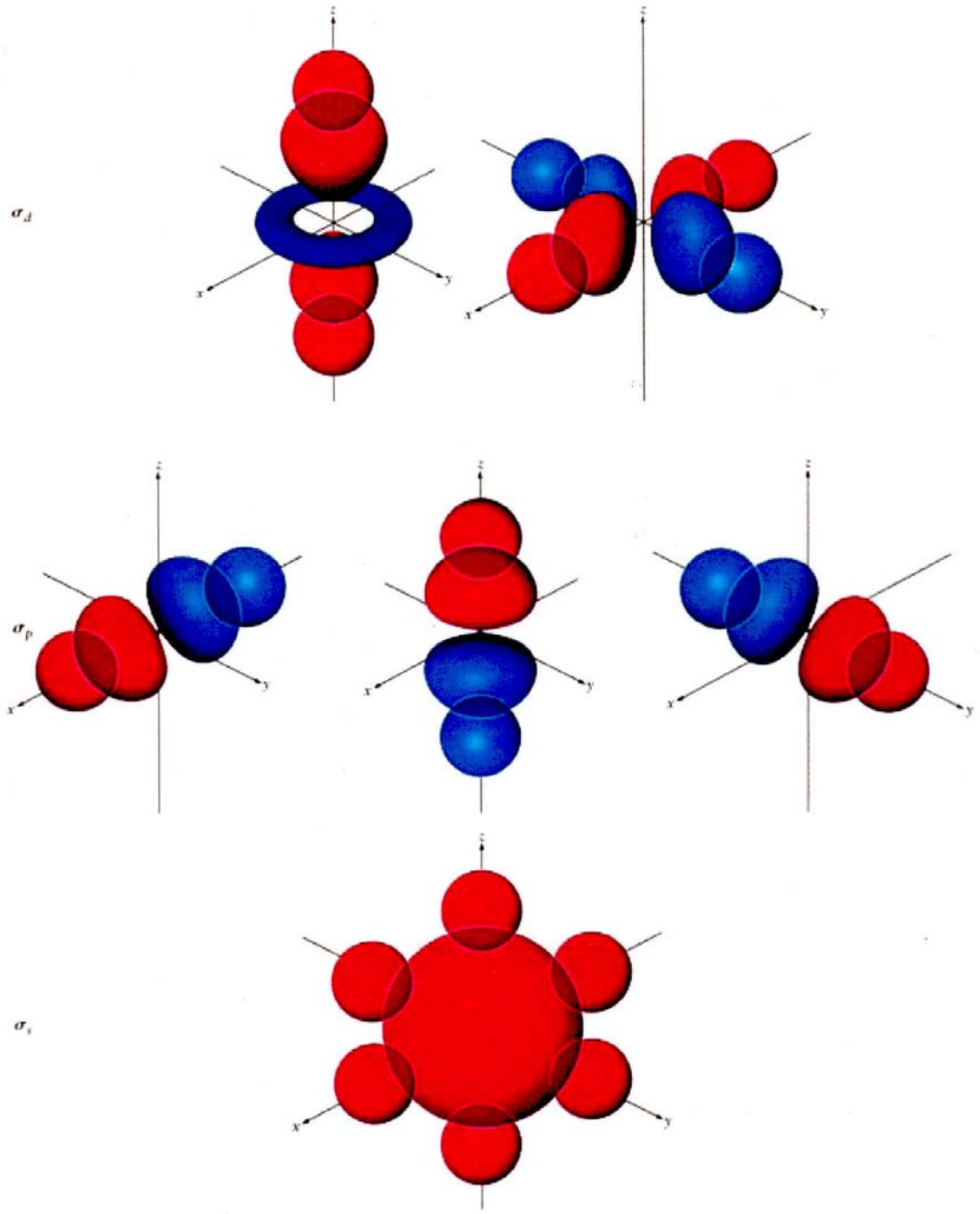

FIGURE 8.32 Overlap of metal orbitals with ligand orbitals to form σ bonds. The ligand orbitals can be either p or hybrid orbitals (e.g., sp^3 for water), and thus they are represented only schematically.

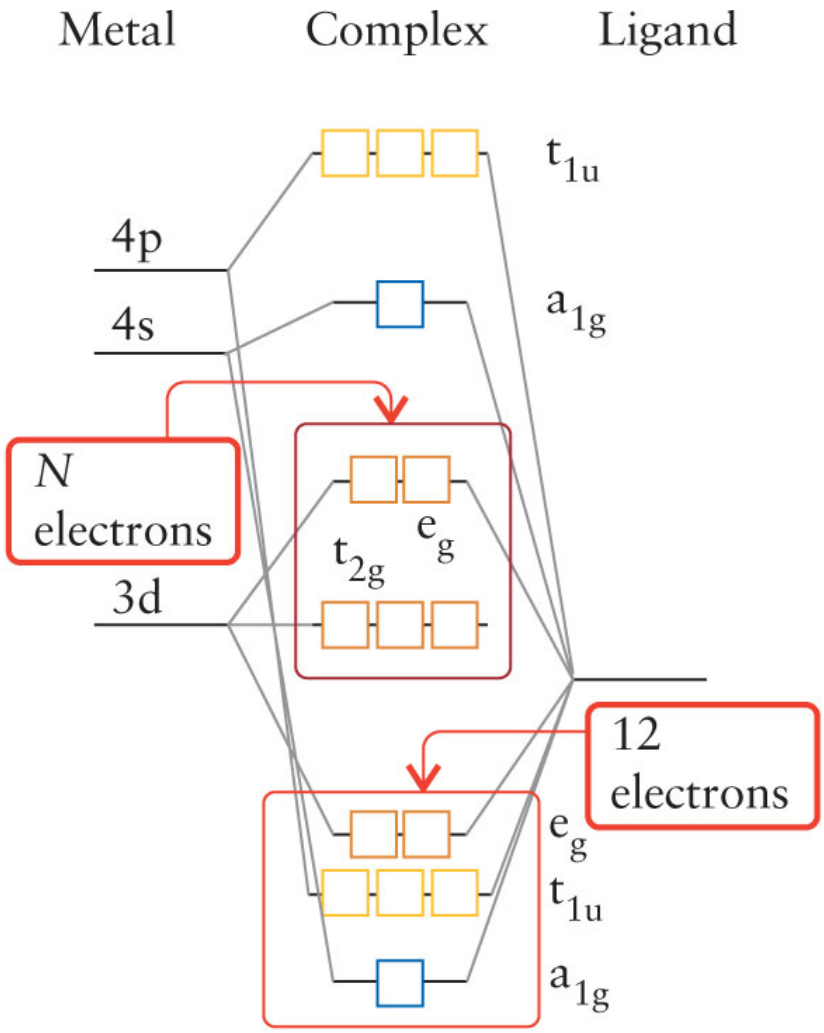

FIGURE 17.40 The molecular orbital energy-level diagram for an octahedral complex. The 12 electrons provided by the six ligands fill the lowest six orbitals, which are all bonding orbitals. The *N* d-electrons provided by the central metal atom or ion are accommodated in the orbitals inside the upper box. The ligand field splitting is the energy separation of the nonbonding (t_{2g}) and antibonding (e_g) orbitals in the box.

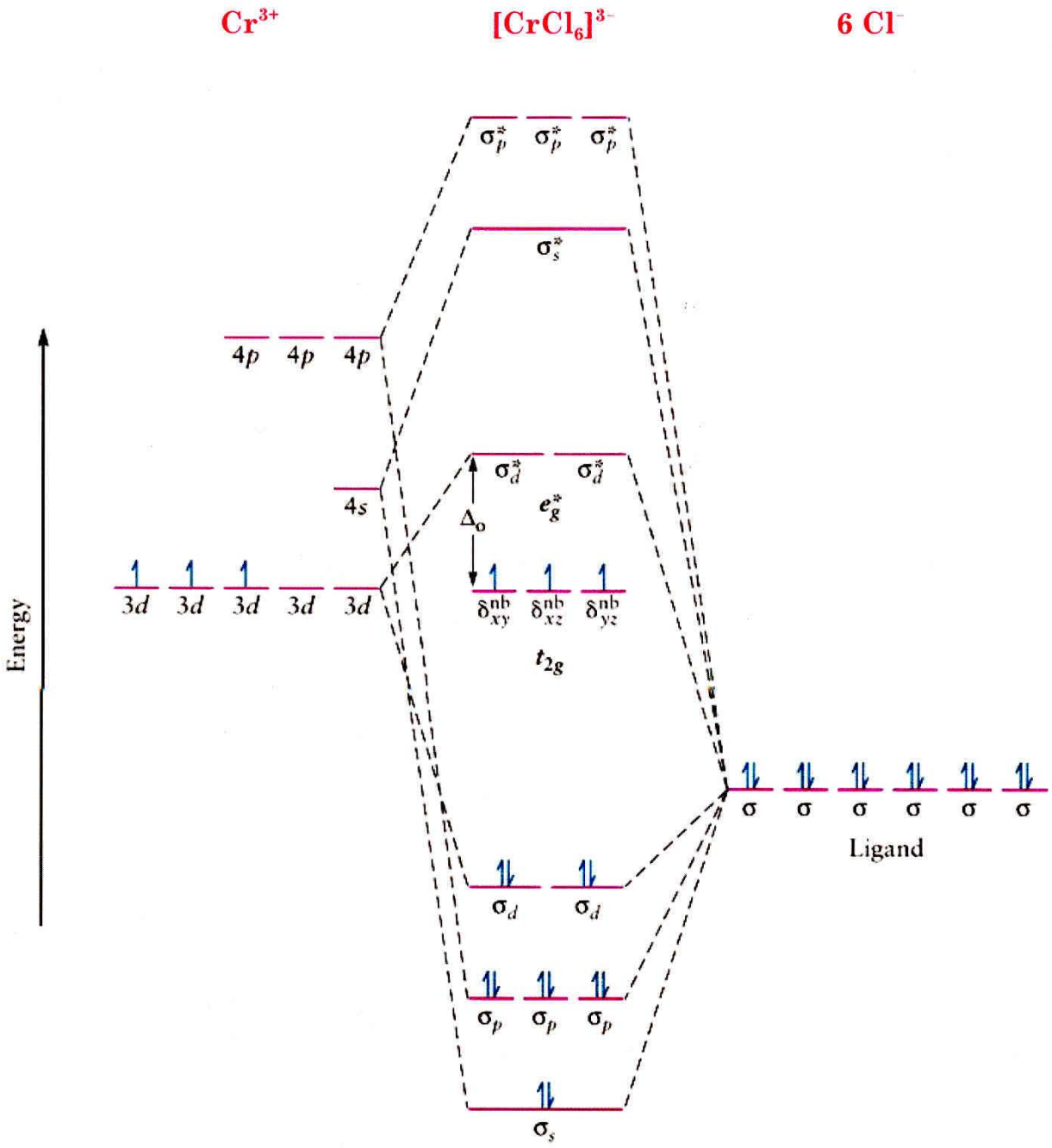

FIGURE 8.33 Orbital correlation diagram for an octahedral ligand field, showing the energy-level filling for a $[CrCl_6]^{3-}$ ion.

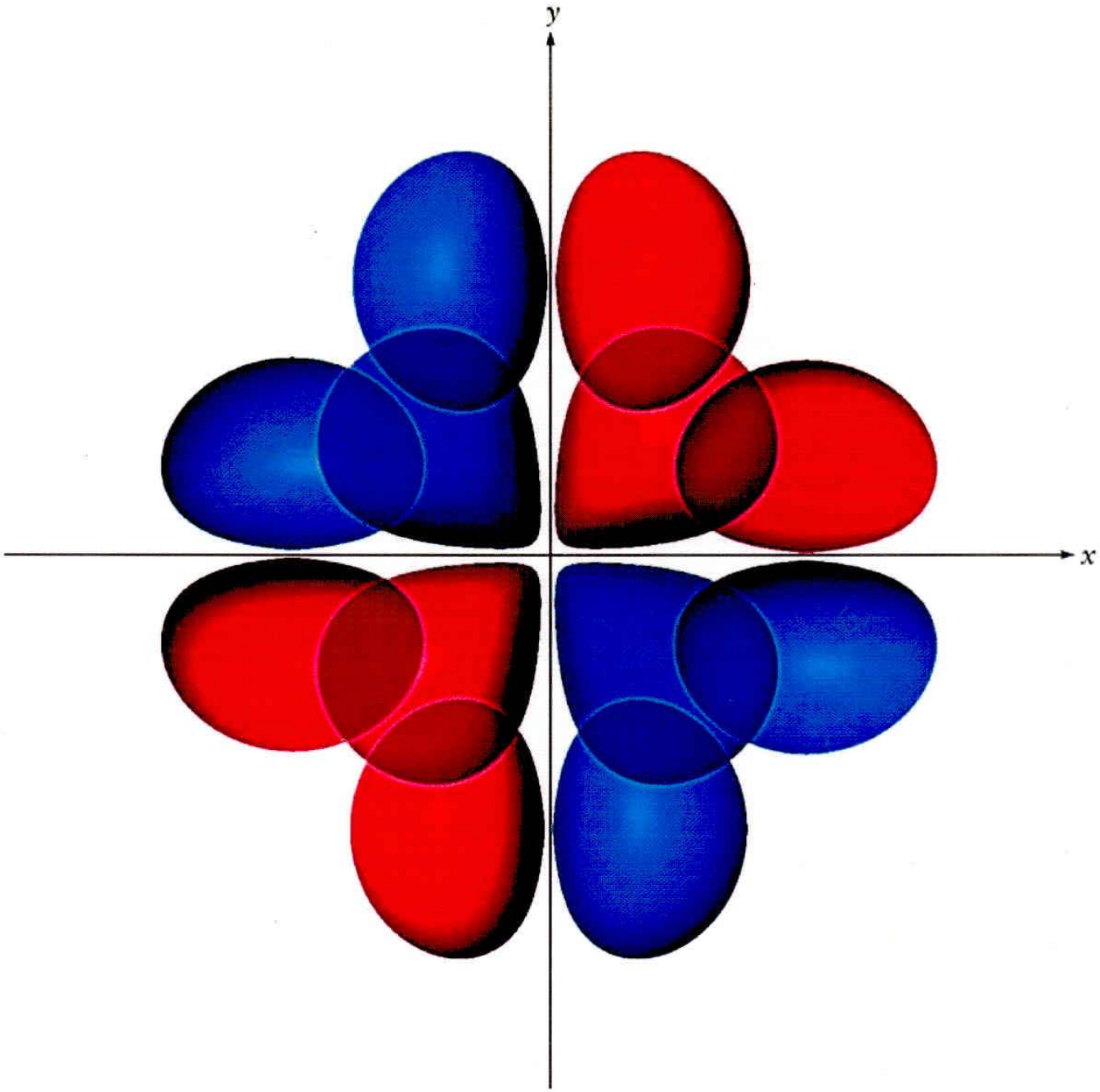

FIGURE 8.34 π bonding between a metal d_{xy} orbital and four ligand π orbitals with phases chosen for maximum constructive overlap.

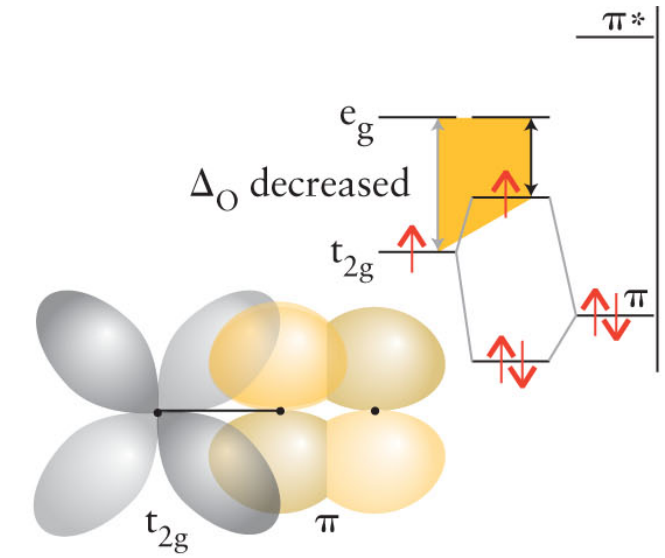

(a)

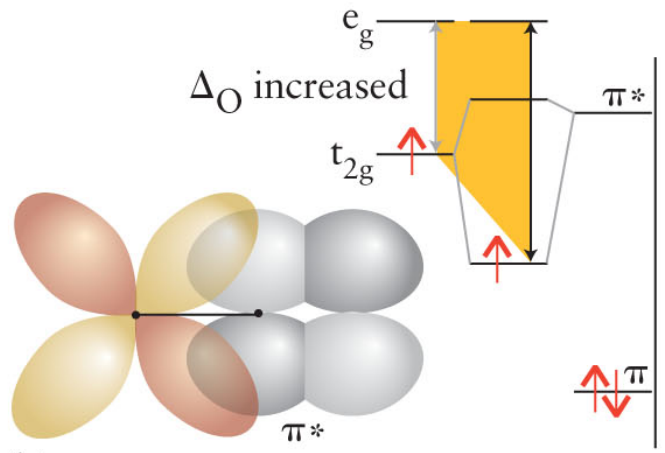

(b)

FIGURE 17.41 The effect of π-bonding on ligand field splitting. (a) In this case, the occupied π-orbital of the ligand is close in energy to the metal t_{2g} orbitals and they overlap to form bonding and antibonding combinations. The ligand field splitting is reduced. (b) In this case, the unoccupied antibonding π*-orbital of the ligand is close in energy to the metal t_{2g} orbitals and they overlap to form bonding and antibonding combinations. In this case, the ligand field splitting is increased.

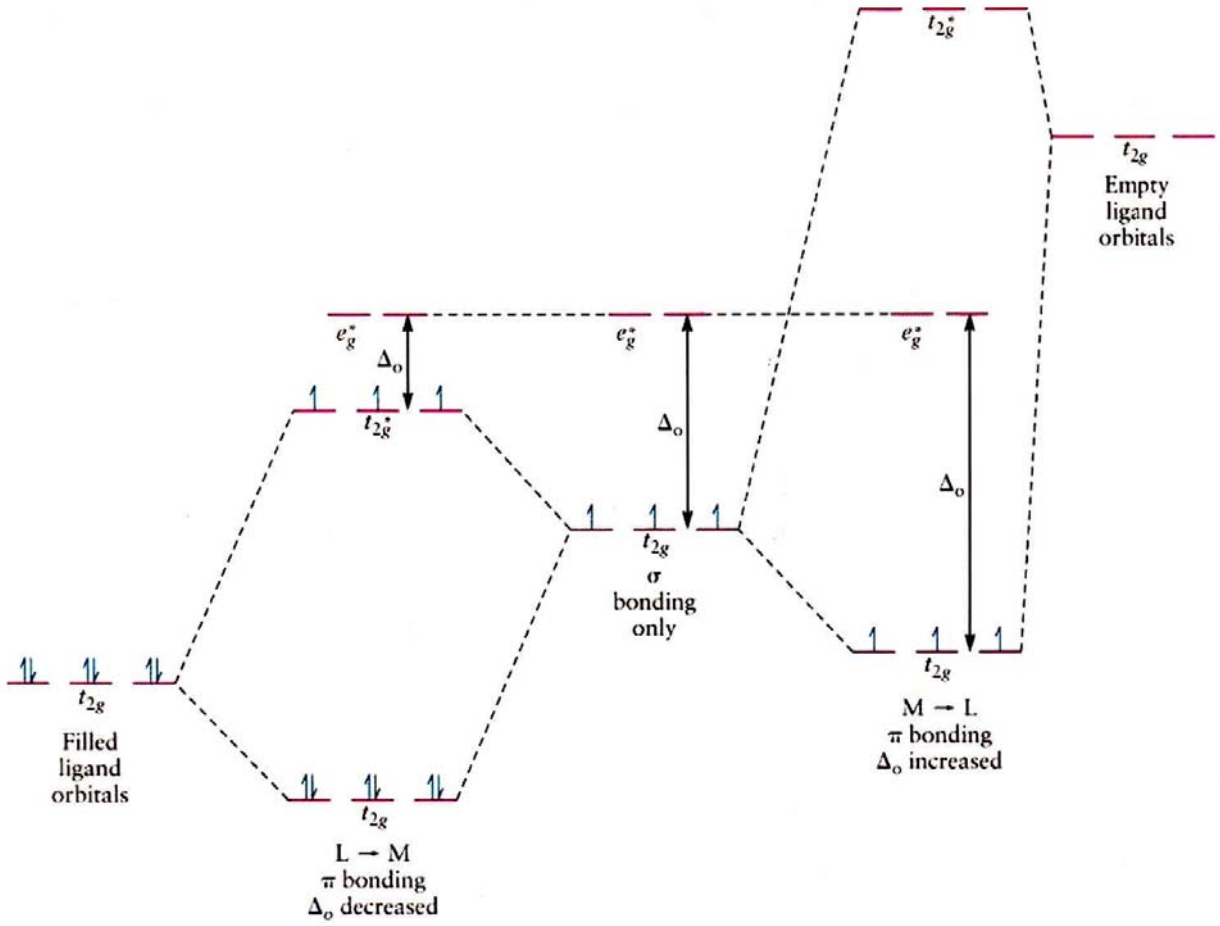

FIGURE 8.35 Effect of π bonding on the energy-level structure for octahedral coordination complexes. The center energy-level diagram is appropriate for intermediate field ligands that are σ donors only. The left energy-level diagram shows how weak field ligands (π donors) decrease Δ_o, and the right energy-level diagram shows how strong field ligands (π acceptors) increase Δ_o.